CRUISE REPORT

Underway Measurements of Essential Marine Biogeochemical Variables in the Arctic

Le Commandant Charcot, Cruise No. : 0623 2022 & 0628 2022,

06/23 – 07/08, Port of mobilisation (Longyearbyen, Svalbard) – Port of demobilisation (Longyearbyen, Svalbard)

Principal Investigators: Brent Else (University of Calgary), Philippe Tortell (University of British Columbia)

Participants: Yayla Sezginer (University of British Columbia), Katrina Schuler (University of British Columbia)

Contents

Summary

Current understanding of the Arctic Ocean's response to climate change is limited by a lack of observational data. Many essential climate variables are rarely measured in the Arctic. Similarly, the Argo float program, which provides in situ measurements of essential climate variables, has no significant presence in the Arctic (Jayne et al, 2017, 10.5670/oceanog.2017.213). One approach to this 'observational hole' is the use of underway sensors aboard ships transiting the Arctic. These instruments sample water continuously from a vessel's seawater intake, providing measurements of physical, chemical, and biological variables along the cruise track. When operating on vessels transiting large spatial extents or conducting repeated voyages along a scheduled route, underway sensors can dramatically increase knowledge of near-surface ocean processes.

One of the biggest questions in Arctic marine ecosystem science is how phytoplankton – the base of the Arctic food web – will respond to sea ice loss. Satellite remote sensing studies have suggested an increase in phytoplankton primary production (Arrigo & van Dijken, 2015, 10.1016/j.pocean.2015.05.002), but underway systems (e.g. Izett & Tortell (2021, 10.1002/lom3.10440)) are a necessary tool for validating satellite primary production algorithms, and providing greater insights into phytoplankton physiology (Sezginer et al., 2021, 10.1371/journal.pone.0256410). Secondly, certain Arctic regions are also an important source of other greenhouse gasses like methane (CH_4) and nitrous oxide (N_2O) and exhibit significant spatial and temporal variability (Fenwick et al., 2017, 10.1002/2016JC012493). During our voyage onboard *Le Commandant Charcot* No. 0623 and 0628, we deployed a suite of underway sensors to address the research questions outlined above (See also: Program Objectives).

1. Research Program/Objectives

To monitor phytoplankton photophysiology and primary productivity underway we deployed:

(i) a O_2/N_2 sensor to determine net community production of photosynthetically derived O_2.

(ii) a Fast Repetition Rate fluorometer (FRRF) to examine phytoplankton physiology and primary productivity. The method exposes water samples to rapid pulses of intense light and analyzes rapid fluorescence "transients" to derive quantitative estimates of photosynthetic parameters, including photochemical quantum yields, and photosynthetic electron transport rates.

To measure greenhouse gas concentrations and determine information surrounding their biogeochemical cycling, we deployed/measured:

(i) A continuous CH_4 and nitrous oxide N_2O gas analyzer (CH_4/N_2O Gas Analyzer, Los Gatos Research) to measure spatial variability and sea-air fluxes of greenhouse gasses along the cruise-track.

(ii) A continuous $\delta^{13}C\text{-}CH_4$, $\delta^{13}C\text{-}CO_2$ gas analyzer (Picarro, G2201-i) to measure isotopic composition of methane and carbon dioxide along the cruise-track.

(iii) Discrete samples of turbidity, salinity, methane, $\delta^{13}C\text{-}CH_4$, $\delta^{18}O$ to determine the relationship between tidewater glacier meltwater and methane concentrations, and methane sources.

2. Narrative of the Cruise

Daily operations:

- Monitoring data health of online underway instruments and took calibration samples.
- Performing blank measurements for the FRRF instrument by measuring the fluorescence signal of seawater filtered through a 0.2 um filter, to be subtracted from subsequent measurements
- Assisting other teams with on-station sample collection duties (mainly the Deoxygenation Project)
- Collect a Photosynthetically Active Radiation (PAR) reading in close proximity to the Solar Radiation instrument installed by the science team led by Vito Vitale. These daily readings were later used for calibration and to convert Solar Radiation measurements to PAR estimates.

Station sampling

- Discrete sampling for CH_4, N_2O, $\delta^{13}C\text{-}CH_4$, $\delta^{18}O$, turbidity and salinity with Niskins and CTD was performed at various stations, with many stations near the termini of tidewater glaciers and in glacier meltwater plumes all around Svalbard.

Pre/Post Cruise Activity

Prior to the cruise, the excitation lamps within the FRRF were all calibrated with a small hand-held PAR meter. The instrument sensitivity and noise level was assessed by measuring de-ionized water and phytoplankton monocultures of known cell densities. The O_2/N_2 sensor was cleaned & calibrated based on comparison with a winkler titration sample collected in-line with the O_2/N_2 sampling stream. The membrane for underway methane/nitrous oxide and $\delta^{13}C\text{-}CH_4$ was cleaned.

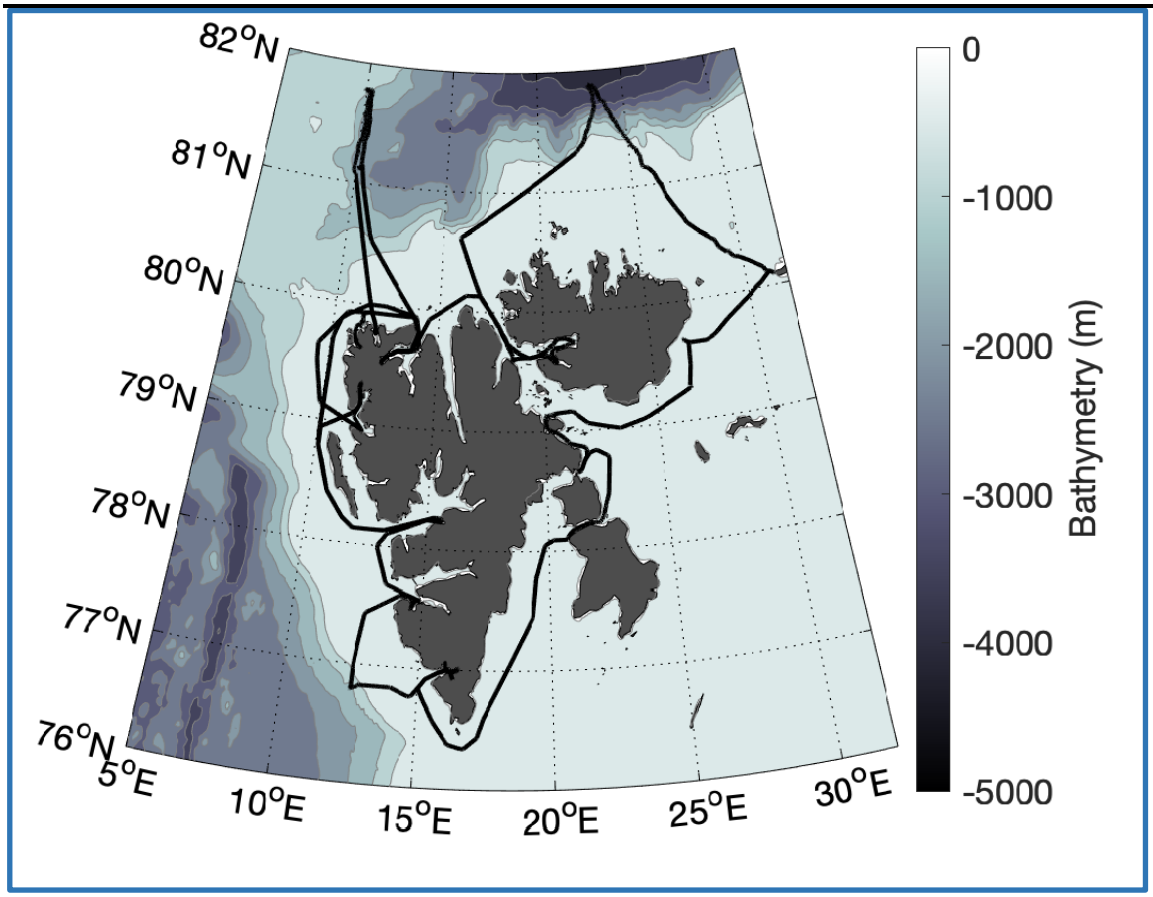

Figure 1. Cruise track of combined legs 0623 and 0628 circumnavigating Svalbard.

3. Station List

Sampling for CH_4, N_2O, $\delta^{13}C$-CH_4, $\delta^{18}O$, turbidity and salinity consisted of deeper/open water stations on the ship, combined with sampling near the face of tidewater glaciers on the zodiac. In the table below, GT = Glacier Terminus, GE = End of fjord/bay and GM= halfway between the two points:

Station No.	Date	Time	Latitude	Longitude	Gear	Remarks/Recovery
		[UTC]	[°N]	[°E]		
S1_06242022	6/24/2022	9:54	79.564	10.99066	Niskin Bottle/CTD	
S2_06262022	6/26/2022	NA	81.075	10.02167	Niskin Bottle/CTD	
S3_06272022	6/27/2022	NA	78.95333	11.895	Niskin Bottle/CTD	
S4_06302022	6/30/2022	11:30	79.84858	10.33593	Niskin Bottle/CTD	
S5_07012022	7/1/2022	1:00	79.88135	17.90443	Niskin Bottle/CTD	

S6_07022022	7/2/2022	12:15	81.88133	23.01499	Niskin Bottle/CTD	
S7_07032022	7/3/2022	1:32	80.35652	29.38545	Niskin Bottle/CTD	
S8_07032022	7/3/2022	20:30	79.2722	26.59466	Niskin Bottle/CTD	
S9_07062022	7/6/2022	3:20	76.97561	15.74695	Niskin Bottle/CTD	
S10_07062022	7/6/2022	20:11	76.82942	12.83354	Niskin Bottle/CTD	
G1T	06/24/2022	NA	79.54235	10.9576	Niskin Bottle/CTD	
G1M	06/24/2022	NA	79.55992	10.95758	Niskin Bottle/CTD	
G1E	06/24/2022	NA	79.57959	10.7852	Niskin Bottle/CTD	
G2E	06/24/2022	NA	79.62635	12.92147	Niskin Bottle/CTD	
G2M	06/24/2022	NA	79.57399	12.65792	Niskin Bottle/CTD	
G2T	06/24/2022	NA	79.53432	12.54656	Niskin Bottle/CTD	
G3E	6/26/2022	NA	79.77333	11.9867	Niskin Bottle/CTD	
G3M	6/26/2022	NA	79.70898	12.07165	Niskin Bottle/CTD	
G3T	6/26/2022	NA	79.65547	12.0745	Niskin Bottle/CTD	
G4E	6/27/2022	NA	79.30603	11.66331	Niskin Bottle/CTD	
G4M	6/27/2022	NA	79.33444	11.64937	Niskin Bottle/CTD	
G4T	6/27/2022	NA	79.35413	11.71826	Niskin Bottle/CTD	
G5T	06/30/2022	NA	79.52148	12.46576	Niskin Bottle/CTD	
G5M	06/30/2022	NA	79.54137	12.5019	Niskin Bottle/CTD	
G5E	06/30/2022	NA	79.57295	12.60927	Niskin Bottle/CTD	
G6T	7/1/2022	NA	79.59115	18.4493	Niskin Bottle/CTD	

G6M	7/1/2022	NA	79.59038	18.55652	Niskin Bottle/CTD	
G6E	7/1/2022	NA	79.57956	18.75997	Niskin Bottle/CTD	
G7E	7/3/2022	NA	80.0758	31.22212	Niskin Bottle/CTD	
G7M	7/3/2022	NA	80.09964	31.37346	Niskin Bottle/CTD	
G7T	7/3/2022	NA	80.1236	31.483	Niskin Bottle/CTD	
G8T	7/3/2022	NA	79.70372	26.53062	Niskin Bottle/CTD	
G8M	7/3/2022	NA	79.69955	26.55012	Niskin Bottle/CTD	
G8E	7/3/2022	NA	79.68694	26.62844	Niskin Bottle/CTD	
G9E	7/4/2022	NA	79.12686	20.28045	Niskin Bottle/CTD	
G9M	7/4/2022	NA	79.11468	20.28379	Niskin Bottle/CTD	
G9T	7/4/2022	NA	79.10836	20.24444	Niskin Bottle/CTD	
G10E	7/5/2022	NA	78.05009	20.75879	Niskin Bottle/CTD	
G10M	7/5/2022	NA	78.0637	20.85197	Niskin Bottle/CTD	
G10T	7/5/2022	NA	78.06805	20.8759	Niskin Bottle/CTD	
G11T	7/6/2022	NA	77.10276	15.77919	Niskin Bottle/CTD	
G11M	7/6/2022	NA	77.063	15.82904	Niskin Bottle/CTD	
G11E	7/6/2022	NA	77.01461	15.91759	Niskin Bottle/CTD	
G12T	7/6/2022	NA	77.09789	15.76599	Niskin Bottle/CTD	
G13E	7/7/2022	NA	77.50629	14.69434	Niskin Bottle/CTD	
G13M	7/7/2022	NA	77.49057	14.72164	Niskin Bottle/CTD	
G13T	7/7/2022	NA	77.4811	14.75218	Niskin Bottle/CTD	

4. Preliminary Results

4.1 Primary Productivity

4.1.1 O_2/N_2

We observed distinct spatial variability in the $\Delta O_2/N_2$ signature surrounding the Svalbard Archipelago (Figure 2). This metric describes the % deviation in dissolved O_2 concentrations from theoretical values calculated based on temperature and salinity effects on O_2 solubility. These deviations represent the net effects of photosynthesis – respiration and thus represent net community productivity (NCP). To the southeast of the Archipelago, NCP was high while the Northwest end displayed lowed NCP with oxygen levels close to saturation. Differences in NCP are ultimately influenced by differences in phytoplankton growing conditions and the availability of growth limiting factors such as nutrients and light. In this case, the West Spitsbergen Current, which carries warm, saline Atlantic water north along the NW end of Svalbard and the East Spitsbergen Current carrying cold and fresh Arctic water south along the SE end of Svalbard are likely driving the observed spatial heterogeneity in NCP.

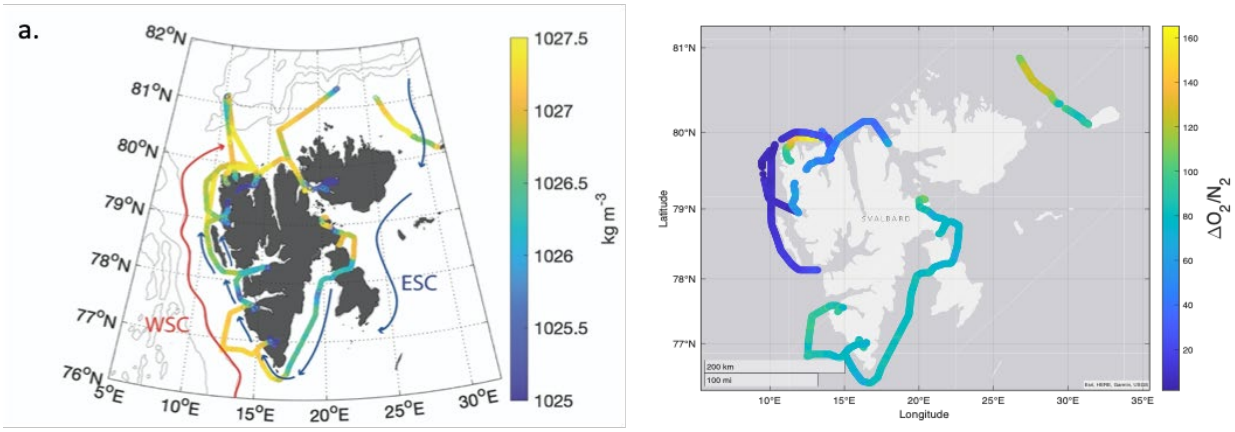

Figure 2. a. Displays the seawater density determined from the underway Seabird 45 TSG system to illustrate the distinct water masses present attributed to the West Spitsbergen Current and the East Spitsbergen Current. Arrows indicated the movement of the water masses were adapted form Vihtakari et al. (2019). B. Underway O_2/N_2 surrounding the Svalbard Archipelago. Gaps in the data set occurred when the underway pump was turned on in the presence of sea ice.

4.1.2 Fast Repetition Rate Fluorometry

Two core measurements provided by FRRF analysis are the maximum photochemical yield of Photosystem II (F_v/F_m) and the functional absorption area of Photosystem II (σ_{PSII}). Respectively, these measurements represent the fraction of absorbed photons that are used to drive photosynthetic electron transport and the relative size of photosynthetic light harvesting complexes. These photophysiological parameters dictate the efficiency with which light energy is converted to photochemical energy, which in turn provides an upper limit for downstream carbon fixation and other metabolic functions. The σ_{PSII}, in particular showed significant E-W variability. Different phytoplankton taxa have unique light harvesting pigment compositions, causing the functional PSII absorption area, σ_{PSII}, to show taxon-specific variability (Suggett *et al.*, 2009; Gorbunov *et al.*, 2020). Although F_v/F_m also varies with species composition, it is more strongly affected by

nutrient concentrations, and is thus widely used as an indicator of environmental conditions (Ryan-Keogh *et al.*, 2013; Ko *et al.*, 2020). The significant differences we observed in σ_{PSII} but not Fv/Fm suggest variability between subregions of the Svalbard Archipelago are due to changes in taxonomic composition, rather than direct environmental effects (i.e. nutrient abundance).

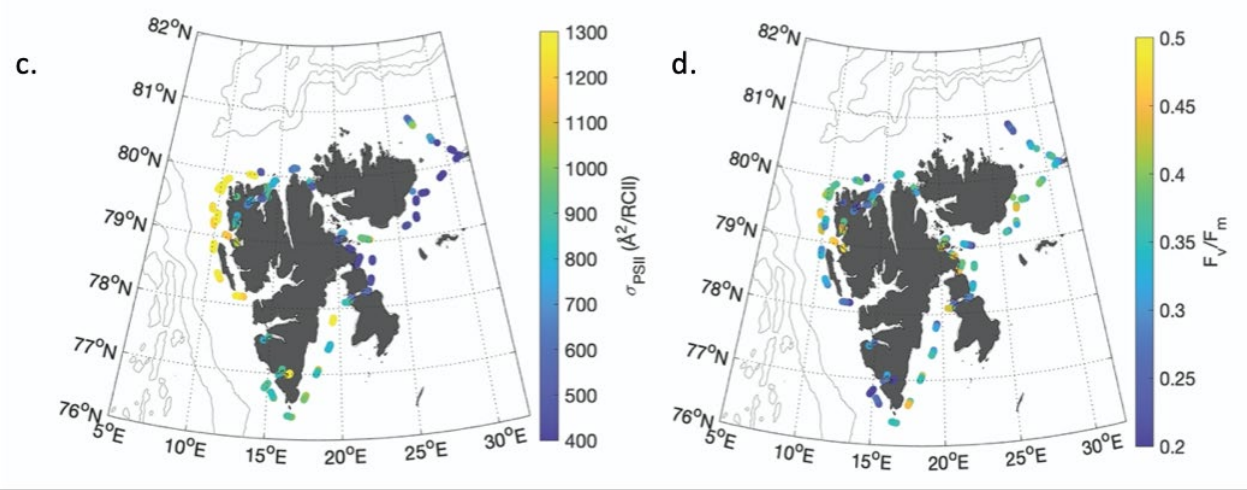

Figure 3. a) the functional PSII absorption area, σ_{PSII}, was high in the W with values typical of haptophytes, and low in the E with values matching those of chlorophytes (Gorbunov et al., 2020). B. There was less apparent E-W variability in Fv/Fm.

4.2 Gases

4.2.1 Underway data

Underway methane data was variable throughout the cruise, with notable hotspots in fjords (Raudfjorden and Hornsund fjord) and near Cape Payer. Calibration samples showed good agreement with the continuous data measured from the seawater supply line (Fig. 5).

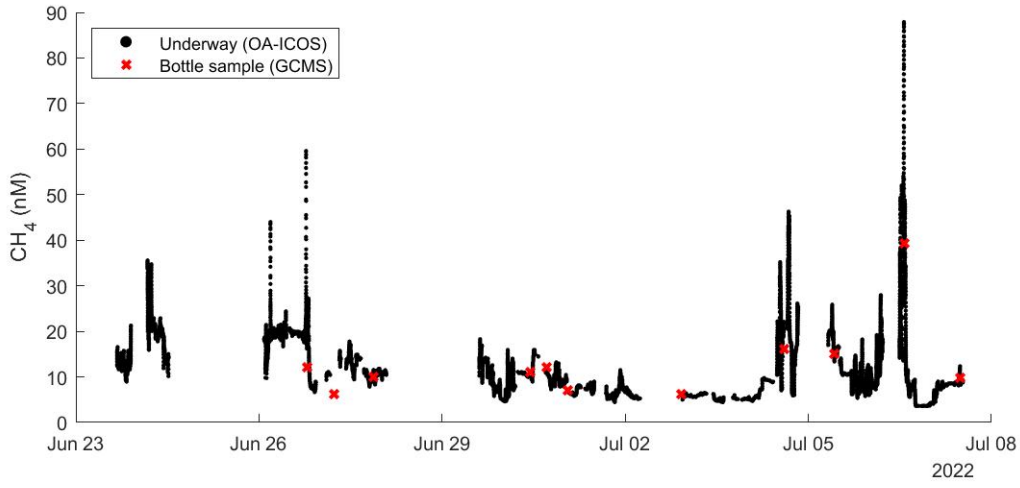

Figure 4. Calibrated time series of underway methane concentration.

Elevated methane concentration observed in the vicinity of Cape Payer is shown in Fig. 5. Underway data was plotted over satellite imagery and showed significant overlap between elevated concentration and turbid plumes coming from land, suggesting a land-based source of methane.

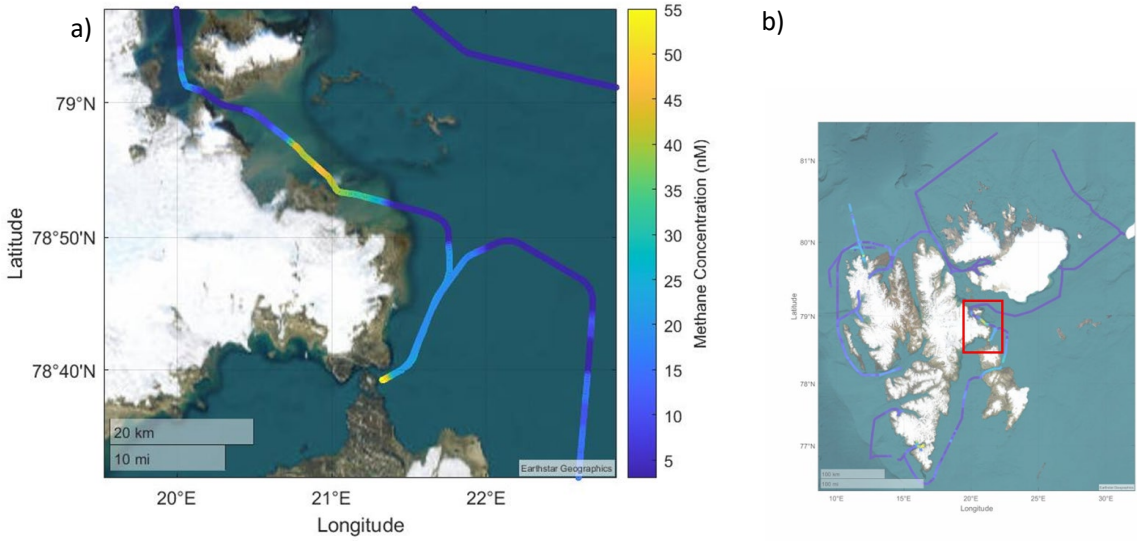

Figure 5. Methane hotspots on the east coast of Svalbard (a). The location of zoom in (a) is shown in (b).

Temperature & salinity data show that the methane peaks are associated with relatively fresher water (Fig 6a). The methane peaks near Cape Payer also exhibit δ^{13}C-CH_4 values in the range of -50 to -70 permil, indicating that the source of the methane may be microbial, not thermogenic (Fig 6b).

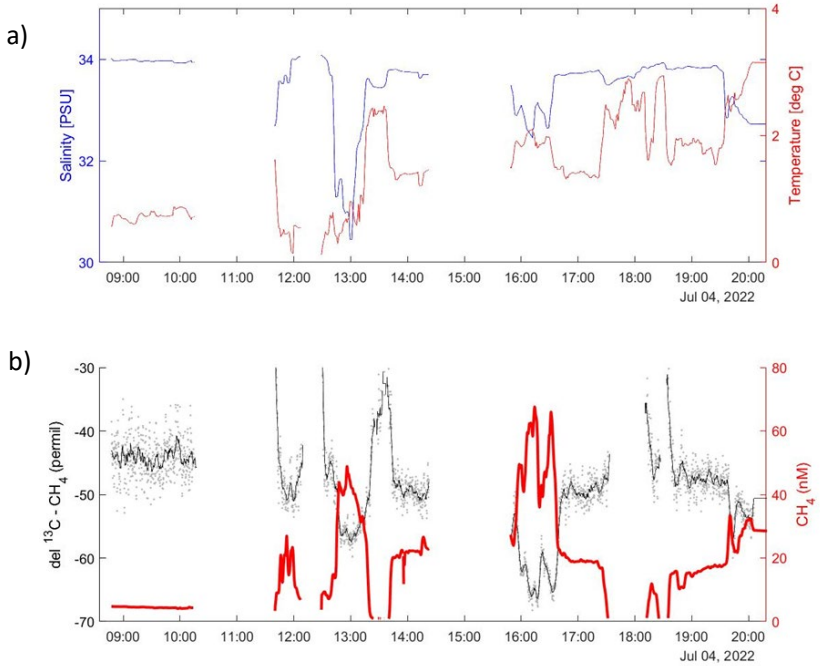

Figure 6. Temperature/Salinity (a) and Methane/δ^{13}C-CH_4 (b) concentration for the two hotspots shown in Fig. 5.

The highest methane concentration observed in the underway data was in the east end of Hornsund Fjord (Fig. 7a & b). There was a less obvious relationship with salinity in this case, i.e. higher methane was not necessarily associated with fresher water (Fig 7b). Additionally, the isotopic signature was notably heavier than previous hotspots (-40 permil), suggesting a potentially thermogenic source in this location.

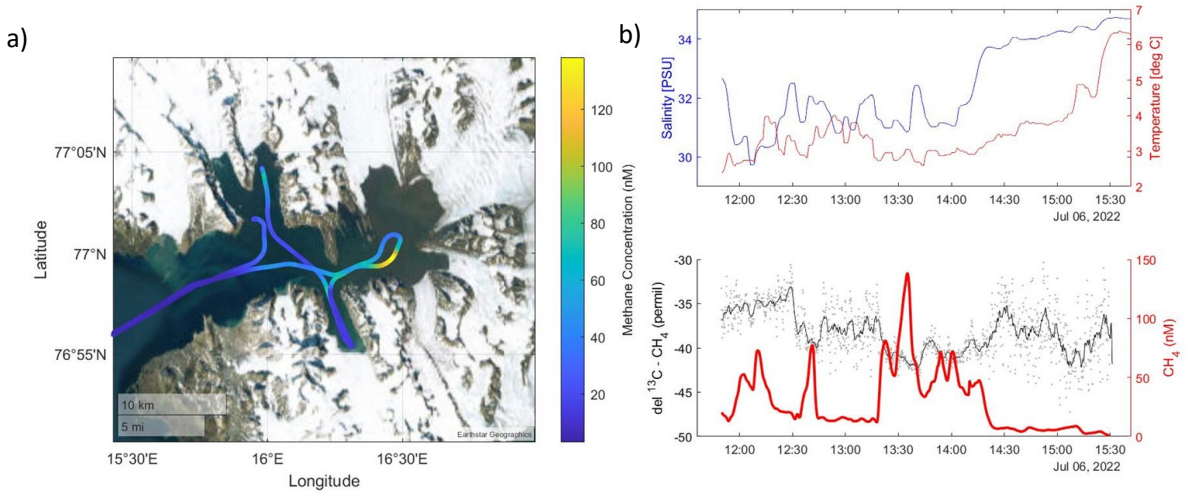

Figure 7. Methane hotspot in Hornsund Fjord (a). Underway temperature/salinity data and methane/δ^{13}C-CH_4.

These two distinct sources of methane are further exemplified in Fig. 8, which shows the points of each hotspot lying along two distinct Rayleigh fractionation curves. These curves provide evidence for the occurrence of methane oxidation in the water column in both locations.

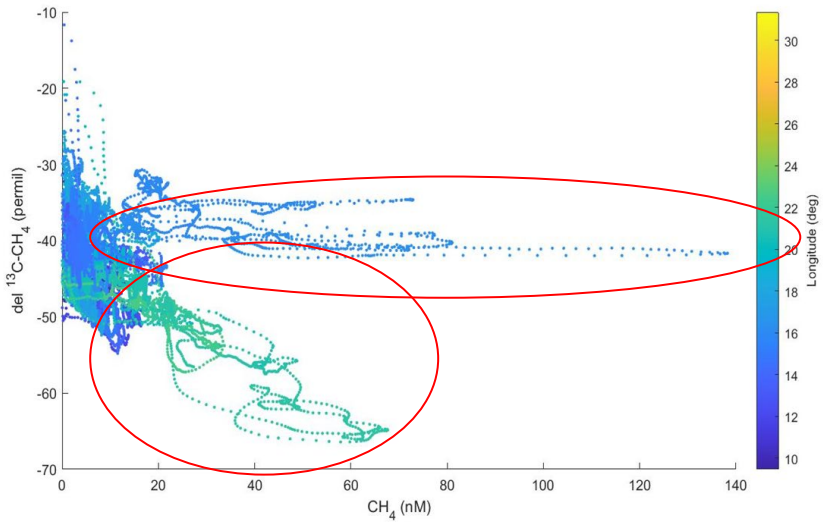

Figure 8. Scatter plot of δ^{13}C-CH_4 vs. methane concentration shows two distinct sources for each of the hotspots shown in figures 5 and 7.

5. Data and Sample Storage / Availability

Data is preliminary and has not been submitted to an online database, but will be submitted to a database, hosted by Pangaea by Dec 2023.

6. Participants

No.	Name	Early career (Y/N)	Gender	Affiliation	On-board tasks
1	Yayla Sezginer	Y	F	UBC	FRRF sampling
2	Katrina Schuler	Y	F	UBC	Trace Gas sampling

UBC University of British Columbia

7. Acknowledgements

The authors would like to acknowledge PONANT for in kind contribution and their science coordinators for scientific logistical field support while on board. We would also like to acknowledge ARICE, EU grant agreement No. 730965 which helped make this field work possible.

8. References

Fenwick, L., Capelle, D., Damm, E., Zimmermann, S., Williams, W. J., Vagle, S., & Tortell, P. D. (2017). Methane and nitrous oxide distributions across the North American Arctic Ocean during summer, 2015. *Journal of Geophysical Research: Oceans*, *122*(1), 390–412. https://doi.org/10.1002/2016JC012493

Gorbunov, M. Y. *et al.* (2020) 'A multi-spectral fluorescence induction and relaxation (fire) technique for physiological and taxonomic analysis of phytoplankton communities', *Marine Ecology Progress Series*, 644, pp. 1–13. doi: 10.3354/meps13358.

Ko, E. *et al.* (2020) 'Effects of Nitrogen Limitation on Phytoplankton Physiology in the Western Arctic Ocean in Summer', *Journal of Geophysical Research: Oceans*, 125(11), pp. 1–19. doi: 10.1029/2020JC016501.

Ryan-Keogh, T. J. *et al.* (2013) 'Spatial and temporal development of phytoplankton iron stress in relation to bloom dynamics in the high-latitude North Atlantic Ocean', *Limnology and Oceanography*, 58(2), pp. 533–545. doi: https://doi.org/10.4319/lo.2013.58.2.0533.

Suggett, D. J. *et al.* (2009) 'Interpretation of fast repetition rate (FRR) fluorescence : signatures of phytoplankton community structure versus physiological state', 376, pp. 1–19. doi: 10.3354/meps07830.

Vihtakari, M., Sundfjord, A. and de Steur, L. (2019) 'Barents Sea Ocean-Current Arrows Modified from Eriksen et al. (2018)', *Tromsø: Norwegian Polar Institute and Institute of Marine Research*.